Materials Chemistry Horizons RESEARCH

Rapid Adsorption Mechanism of Methylene Blue onto a Porous Mixed Ti-Nb Oxide

Tahmina Akter[1]*, Jose L. Bañuelos[2], Daniel Andrade[1], Dante I. Bañuelos[1], Geoffrey B. Saupe[1]*

[1] Department of Chemistry and Biochemistry, the University of Texas at El Paso, El Paso, TX 79968-0513, USA
[2] Department of Physics, University of Texas at El Paso, El Paso, TX 79968-0513, USA

Corresponding authors: takter@miners.utep.edu (T. Akter); gsaupe@utep.edu (G. B. Saupe)

Mater. Chem. Horizons, 2022, 1(1), 49-67 10.22128/mch.2022.555.1006 OPEN ACCESS

ABSTRACT

This study explores the incorporation of aqueous methylene blue (MB^+) into a specially prepared metal oxide host. Derived from the chemical exfoliation of $KTiNbO_5$ into nanosheet colloids, the host material was synthesized in water using acid to restack the colloids into aggregates of nanosheets. The metal oxide host has a large open pore, disordered, and turbostratic layered structure. When exposed to aqueous solutions of MB^+, within minutes the novel host rapidly intercalated MB^+ to saturation, to produce an organic-inorganic composite with an MB^+ loading of 226 mg/g. Well-rinsed composites exhibited a deep purple color, indicative of the high internal content of MB^+. The MB^+ loading was quantified using EDX and UV-Vis spectrophotometry. Small-angle x-ray scattering (SAXS) measurements were carried out and analyzed using a unified exponential/power-law (UEP) model to describe the composite's nanostructure. SAXS analyses indicated that intercalated material is composed of two phases, each with different layer spacings for the restacked sheets. Compared to transmission spectra of aqueous MB+, diffuse reflectance UV-Vis absorption spectra of composite revealed changes in the absorbance maxima of the intercalated MB^+, indicating that the MB^+ molecules were interacting strongly with each other and with the oxide host. Raman and IR spectra also revealed significant host-guest interactions. As determined by x-ray diffraction, the measured layer spacing between restacked nanosheets in the composite is consistent with a molecular orientation of MB^+ standing on the end but tilted 40.4° away from the plane of the sheets. Electron microscopy analysis showed that there were no significant morphological changes occurred in the porous host aggregates during the intercalation of MB^+. From an electrostatics evaluation, the new organic-inorganic composite materials were found to contain 40 % of the theoretical maximum of MB^+, which resulted in an empirical formula of $(MB)_{0.4}H_{0.6}TiNbO_5$.

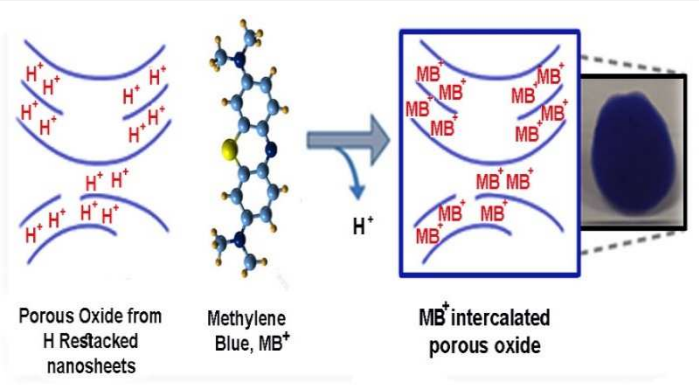

Keywords: Methylene blue, intercalation, restacked, porous, $KTiNbO_5$, SAXS

1. Introduction

Many materials have been studied as hosts or absorbents for dye compounds. Host materials include dry plant biomass, activated carbons derived from biomass, graphitic carbons, polymers, clays, and other solids with a layered structure [1]. Due to their potential as high capacity hosts, stability, and possible catalytic properties, layered metal oxide materials have also generated much interest for the incorporation of dyes [2]. There are numerous reports of clays being used to absorb or intercalate organic dyes [3]. In addition, many-layered transition metal oxides are ion exchangeable, and ionic dyes can be loaded into these materials via intercalation methods [4,5]. The intercalation of dyes into the interlayer regions of layered materials can produce interesting dye-host interactions and dye-dye interactions, which can alter the photo-physical properties of the dyes and may even improve the retention of the dyes and the loading capacity of the host [6]. Layered material-dye composites have also been explored as sensor materials, electrocatalytic films, and photocatalysts [7].

Received: Jun 06 2022
Received in revised: June 19, 2022
Accepted: July 16, 2022

Methylene blue, MB^+ (see **Figure 1**), is a water-soluble cationic dye molecule that has been used in the field of therapeutic medicine, as a stain in biological tissue analysis, and as a DNA intercalant [8-10]. MB^+ is also used in industrial processes, often as a dye for textile, paper, leather, and hair colorants [11]. MB^+ has been explored as an electron transfer mediator in thin-film electrode systems [12], and thin films of layered transition metal oxides with intercalated MB^+ have also been explored [13-15]. The absorption or intercalation of MB^+ into various other materials has also been investigated [16-19]. For monomeric MB^+, the molar absorptivity at 664 nm is very high, at 95000 $mol^{-1}cm^{-1}$ [20]. However, in aqueous solutions, it is known that a fraction of the dissolved MB^+ spontaneously forms dimers, which produce a new absorption peak at 605 nm in the UV-Vis transmission spectrum [21].

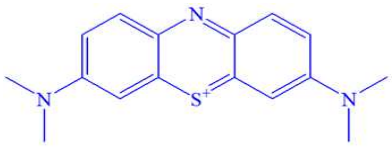

Figure 1. The molecular structure of methylene blue, (methylthioninium, MB^+).

Typically, intercalations of layered materials via ion exchange are accomplished using concentration gradients to drive the exchanges. However, due to size and low charge density factors, the direct intercalation of MB^+ into layered metal oxides is difficult [22]. Even with the aid of pre-expansion intercalation as an intermediate step, others have found that the intercalation of MB^+ into layered $KTiNbO_5$ or KNb_3O_8 took about two weeks to reach equilibrium [15].

To address the drawbacks of direct intercalation methods, our research group and others have been exploring the formation of new intercalated materials, made possible by the restacking of aqueous colloids of ionic nanosheets derived via the exfoliation of layered oxides [23-27]. This interesting approach can form new composite layered materials that are not possible via conventional intercalation routes [23,28]. The restacking process creates new turbostratic layered materials full of disorder, which produces voids and pores in the restacked solid. The resulting porosity gives rise to greatly increased surface areas. The cations used to restack anionic nanosheets end up sandwiched between the restacked nanosheets, thus forming part of the pore walls of the new materials. The ionic nature of the building blocks in the restacking process generally gives the new restacked materials the ability to exchange their cations with those in the surrounding medium [23,29]. This approach permits tailoring materials to contain active components within their nanostructure. So far, there have been only two reports in the literature where the cationic character of methylene blue (methylthioninium, MB^+) was used to induce the restacking of nanosheet colloids to form an intercalated composite material. One report explored MB^+ restacked $K_4Nb_6O_{17}$ as a visible light photocatalyst and photoelectrode, however, the restacked composite was not stable during measurements, and MB^+ de-intercalated into solution [22]. The other report investigated MB^+ restacked $KCa_2Nb_3O_{10}$ as an electrocatalyst material [30].

In the present study, the restacking of nanosheets using methylene blue is not attempted. Instead, we have explored a new way to address the disadvantages of direct intercalation methods. Here we present a novel two-step process, which requires (1) the preparation of a special restacked precursor host material, and (2) the host material is subsequently intercalated by MB^+ via ion exchange. The new porous host is especially easy to intercalate, due to its special properties. In contrast to the restacking efforts of our other work described above [23], this two-step process does not precipitate (or restack) colloids using the new desired cation, but instead the new process provides a high surface area open-pore host material that appears to have a high affinity for the intercalation of MB^+, even at low concentrations.

In this report, we observed an unusually rapid intercalation behavior of MB^+ into a specially prepared ion exchangeable porous metal oxide host. The host is made by chemically exfoliating $KTiNbO_5$ into aqueous nanosheet colloids, followed by restacking the colloids into porous aggregates using acid to create an ion-exchangeable acidic porous oxide (HPOX). It was anticipated that the disordered and open porous structure of the host material would greatly speed up mass transport and facilitate ion exchange. Surprisingly, the new HPOX material had a very high affinity for MB^+, even from solutions in which the concentration of MB^+ was below 50 ppm. The high affinity of the

new HPOX host for MB^+ is interesting, as it is not driven by a concentration gradient or charge density but is likely driven by host-guest interactions and significant guest-guest interactions. To the best of our knowledge, the use of acid-restacked $KTiNbO_5$ colloids to make a porous host material for the intercalation of MB^+ has not been reported. The synthetic methodology reported here has general applicability and could easily be adapted to make other interesting composites.

2. Experimental

2.1. Synthesis of $KTiNbO_5$

The synthesis of potassium titanium niobium pentoxide ($KTiNbO_5$) was based on a conventional solid-state method [23,31]. Reagent grade potassium carbonate (99.9%, Fisher Chemicals), titanium dioxide (99.5%, Sigma-Aldrich), and niobium(V) oxide (99.9%, Alfa Aesar) were purchased and used as received. $KTiNbO_5$ was prepared by grinding stoichiometric amounts of K_2CO_3, TiO_2 and Nb_2O_5 into fine powders with a mortar and pestle and were mixed together thoroughly. A 10% excess of K_2CO_3 was used to counteract the loss of potassium as an oxide vapor during the heating cycle. The mixture was heated in a crucible in a high-temperature furnace (BF51800 series, Lindberg/Blue, USA) for 20 hours via the following program. The temperature was raised from 20-120 ºC at 10 ºC/minute and held at 120 ºC for 60 minutes. The temperature was then raised to 900° C at a rate of 10 °C per minute and held at 900 ºC for 60 minutes. Finally, the temperature was raised to 1100 °C and held for 20 hours, and was then allowed to cool slowly to 20 °C. The product material, $KTiNbO_5$, was stored at ambient conditions until needed. The solid-state synthesis of the layered KTiNbO5 material is shown in Equation 1.

$$2TiO_2 + Nb_2O_5 + K_2CO_3 \longrightarrow 2KTiNbO_5 + CO_2 \qquad \textbf{Eq. (1)}$$

2.2. Synthesis of $HTiNbO_5$

$HTiNbO_5$ was derived from $KTiNbO_5$, by a solution-based ion exchange process, using 3 g of solid in 200 mL of liquid. Powdered $KTiNbO_5$ was stirred at room temperature in aqueous 4 M HCl for 24 hours. The solid was then separated from the liquid using centrifugation. The wet solid was then re-suspended and stirred again in fresh 4 M HCl for 24 hours. Stirring the solid with fresh acid was done a total of four times. Finally, the solid was rinsed well with pure water before allowing the $HTiNbO_5$ material to air dry at room temperature in an open dish (**Scheme 1**).

Scheme 1. The interlayer K^+ in layered $KTiNbO_5$ is ion-exchanged with H^+ to synthesize layered $HTiNbO_5$.

2.3. Preparation of the nanosheet colloids

Exfoliation of $HTiNbO_5$ was done using 40 % aqueous tetrabutylammonium hydroxide (TBAOH, GFS Chemicals, Columbus, Ohio, USA), added dropwise to a suspension of powdered $HTiNbO_5$ until the pH stabilized at about 9. The individual nanosheets are referred to as $(TiNbO_5^-)_n$. The colloid was stirred for a day with TBAOH added as needed to maintain the pH at 9. The pH was monitored using phenolphthalein as an indicator. The indicator dye helps avoid problems with leaking potassium cations from common pH meter probes, as frequent pH determinations are necessary. The colloid container was covered with rubber-lid to avoid atmospheric CO_2 contamination (**Scheme 2**).

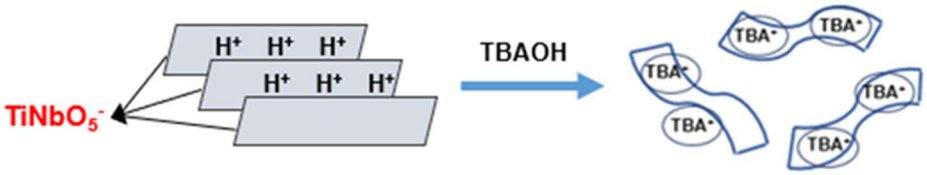

Scheme 2. Exfoliation of $HTiNbO_5$ using TBAOH to make a colloidal solution.

2.4. Synthesis of acid-restacked porous oxide

To make the porous oxide materials, colloids of $(TiNbO_5^-)_n$ at pH 9 or 10 were precipitated by adding 3 mL of 2 M HCl dropwise into 10 mL of the colloid (conc. at 15 mg/mL) while stirring. The H^+ cations precipitate or restack the negatively charged colloidal sheets and create a fluffy white disordered structure. The restacked product was rinsed and washed with pure water until a constant pH of 5 or 6 was achieved. The resulting porous oxide is H^+ restacked $(TiNbO_5^-)_n$ and it is referred to as HPOX. The HPOX was kept wet until used (**Scheme 3**).

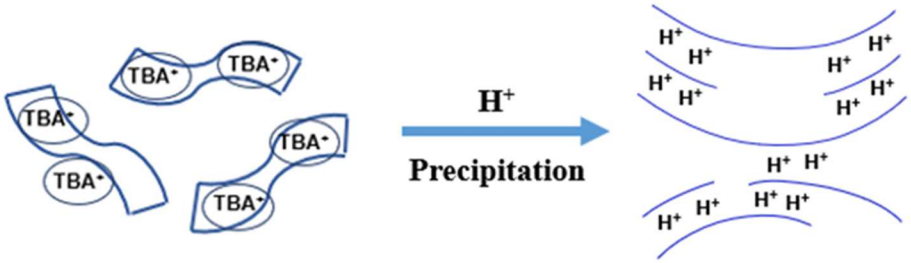

Scheme 3. Precipitation of colloids by adding HCl to make HPOX.

2.5. Intercalation of methylene blue into HPOX and $HTiNbO_5$

While stirring 0.5 mL of water that contained 6.5 mg of HPOX, at approximately - second intervals, 4-5 drops of 50 ppm aqueous methylene blue were added from a burette. The disappearance of the MB^+ was almost instantaneous until the end. MB^+ was added until the supernatant liquid remained blue and the solid did not appear to absorb any more dye (total time approx. 10 min.). At that time, an additional 2 ml of the 50 ppm MB^+ solution was added, and the mixture was allowed to sit overnight. The concentration of MB^+ in the overnight soaking was about 2.5 ppm. After soaking overnight, the resulting MB-loaded porous oxide materials were centrifuged and rinsed many times with pure water until no dye was present (visually) in the rinse water. The MB^+ intercalated porous oxide material is referred to as MB-POX. Quantification of intercalated MB^+ was inferred by analyzing the supernatant solutions and rinse waters. Powdered $HTiNbO_5$ was stirred in 50 ppm solutions of MB^+ for 24 h. After separation, the supernatant was then analyzed with UV-Vis absorption spectrophotometry to estimate the extent of intercalation.

2.6. Small-angle X-ray scattering

Small-angle x-ray scattering (SAXS) measurements were carried out using a Xeuss 2.0 HR SAXS/WAXS system (Xenocs, Sassenage, France) with a Cu source tuned to $\lambda = 0.1542$ nm. Three sample-detector distances (sd) of 156 mm, 1130 mm, and 2400 mm were used to span a Q-range of 0.0032-2.6 $Å^{-1}$. In SAXS, x-rays scattered as a function of the scattering angle 2θ, concerning the transmitted direct beam, are collected on an area detector. The 2-D data is azimuthally averaged and plotted as I(Q). Here, Q is given by $Q = 4\pi\sin\theta/\lambda$, where θ is half the scattering angle, and Q is related to the size of the scattering object d, as $Q \sim 1/d$. To obtain the counting statistics shown in the plots, data was collected for 1800 s at both sd 1130 mm and 2400 mm, and for 600 s at sd 156 mm. Scattering from a water-filled capillary was used as the background measurement and subtracted from the presented data. The SAXS intensity I(Q) was scaled to units of differential scattering cross-section per unit volume (cm^{-1}) using a glassy carbon intensity calibration standard [32]. The HPOX and the MB-POX materials in water were each loaded into 1 mm path length, thin wall, boron-rich, glass capillaries, which were then sealed using beeswax.

2.7. Other characterizations

UV–Vis diffuse reflectance spectrophotometry (UV-Vis-DRS) spectra of the dried MB-POX materials were measured (UV-3101 PC, Shimadzu, Japan). UV-Vis transmission absorption spectra of MB^+ dye solutions were obtained using Cary 300, Cary 50, and Cary 60 spectrophotometers (Varian, USA). Scanning electron microscopy (SEM: Hitachi S-4800, Japan) was used to inspect the morphology of the materials. For the SEM analysis, samples were air-dried and placed on carbon tape for the analyses. Transmission electron microscopy (TEM) was performed with a Hitachi-7650 (Hitachi, Japan) at New Mexico State University under a grant from the National Science Foundation, MRI-DBI-0520956. Energy dispersive x-ray spectroscopy (EDX/EDS: Hitachi S-3400 N) was used to obtain information about the elemental composition of samples. Raman spectra were obtained using a Horiba LabRAM HR Evolution (Horiba; France), where the excitation laser wavelength used was 532 nm, and the samples were air-dried before analysis. Thermogravimetric analyses (TGA/DSC Metler Toledo, Switzerland) were performed in air using a heating rate of 10 °C/min over a temperature range of 25-1000 °C.

3. Results and discussion

$KTiNbO_5$ is a layered metal oxide semiconductor material, well known for the ability to ion exchange its potassium cation for other cations in aqueous solutions [33,34]. Consequently, the synthesis of $HTiNbO_5$ from $KTiNbO_5$ was easily achieved by stirring powdered $KTiNbO_5$ in a series of strong acid solutions to drive the ion exchange process. $HTiNbO_5$ was then exfoliated in water into a colloid of single nanosheets [35], using tetrabutylammonium hydroxide (TBA^+OH^-). Exfoliation occurs via an acid-base neutralization reaction, which consumes the H^+ and forces the bulky TBA^+ in between the oxide layers, promoting the exfoliation of the layers into anionic nanosheets [35]. The metal oxide nanosheets are represented as $(TiNbO_5^-)_n$. The nanosheets are almost 1 nm thick and may extend to lateral dimensions of several microns [36]. Our lab and others have shown that such colloids can be restacked into new materials by introducing suitable cations into the colloid solutions, causing the nanosheets to quickly aggregate into porous low-density solids [35,37,38]. The resulting porosity is a result of the imperfections and disorder caused by the folding and wrinkling of the sheets as they restack, thus forming voids or pores. Here we have induced the restacking of the $(TiNbO_5^-)_n$ colloids with acid, resulting in an acidic porous oxide with H^+ holding the $(TiNbO_5^-)_n$ sheets together through ionic interactions. The combination of H^+ and the $(TiNbO_5^-)_n$ nanosheets in water forms porous $HTiNbO_5$ (or HPOX), which is a stable material (see **Scheme 4**) [23,28,38]. However, HPOX is a porous low-density material and the parent $HTiNbO_5$ is not. Like the parent materials $HTiNbO_5$ and $KTiNbO_5$, HPOX is an ionic layered compound that can be ion-exchanged [23]. Compared with the dense nature of the parent compounds, the open pore high surface area structure of HPOX appears to promote improved mass transport throughout the solid, speeding up ion exchange and other processes [39].

$$KTiNbO_5 + H^+ \rightarrow HTiNbO_5 + K^+$$
$$HTiNbO_5 + TBAOH \rightarrow (TiNbO_5^-)_n\ colloid + H_2O + TBA^+$$
$$(TiNbO_5^-)_n\ colloid + H^+ \rightarrow HPOX$$

Scheme 4. Summary of the synthesis of HPOX starting from $KTiNbO_5$

The synthesized HPOX was explored here as a host for the intercalation of methylene blue in the water. In aqueous solutions, MB^+ is a singly charged cation (see **Figure 1**). In water MB^+ partially self-associates as a cationic dimer $(MB^+)_2$ at concentrations higher than 2.5 x 10^{-6} M due to hydrophobic and dipole interactions [40]. Compared to H^+, MB^+ has a relatively low charge density, due to its larger size. Therefore, it was surprising to find that MB^+ very quickly intercalated into the new HPOX materials in water, displacing the H^+ in the process. While stirring, 3-4 drops of an MB^+ solution were added to the HPOX material at 5 or 10-second intervals, and within seconds of each addition, the blue color of the MB^+ dye in the liquid phase disappeared completely and colored the solid. Even at about 80% of saturation loading, the rate of MB^+ absorption into HPOX was very fast, and the HPOX took only seconds to intercalate the newly added MB^+. The intercalation of MB^+ resulted in a deep blue solid, where the methylene blue was held in the interlayer regions of HPOX. **Figure 2** summarizes the intercalation process. This new MB^+ intercalated HPOX material is referred to as MB-POX. The saturated MB-POX was thoroughly rinsed with pure water before all characterizations.

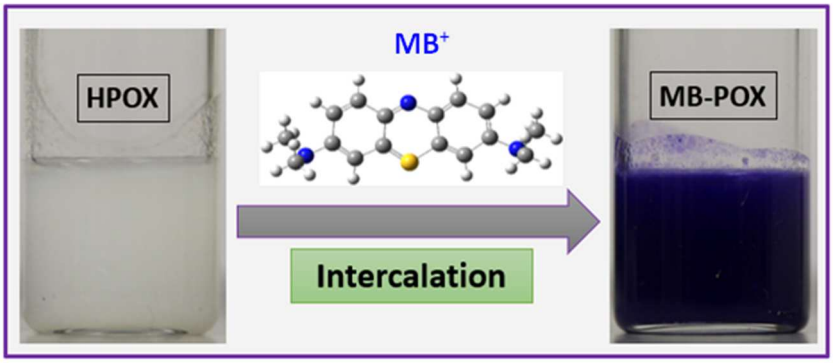

Figure 2. Rapid intercalation of MB^+ into HPOX to produce an organic-inorganic composite saturated with MB^+, MB-POX.

Before considering the results of MB^+ intercalation into HPOX to create MB-POX, some discussion on the common driving forces that enable intercalations will be useful. Typically, the intercalation of ionic layered materials via ion exchange is accomplished using concentration gradients to drive the exchange. This strategy involves soaking the parent compound in fairly concentrated aqueous solutions of the desired ion. The concentration gradient induces the release of the old ion into the solution and the intercalation of the new ion into the solid. Generally, this treatment must be repeated several times with fresh solutions in order to achieve a full exchange of the ions [28]. As in the present work, the ion exchange process used to exfoliate $HTiNbO_5$ is in a special category. The neutralization of the interlayer H^+ ions by the TBAOH resulted in TBA^+ as the only cation available for intercalation into the solid. The resulting electrostatic forces push the large TBA^+ cations into the interlayer regions, expanding the layers, and thus powering the exfoliation process [23]. The low charge density of the intercalated TBA^+ does not fully compensate for the negative charge on the layers of sheets, which leaves the exfoliated sheets with a net negative charge, thus creating a colloidal suspension of sheets.

In some cases, ion exchange processes can also be driven by a substantial difference in the charge densities of the two competing ions, where the higher charge density ion interacts more strongly with the host and can therefore be preferentially intercalated. Therefore, even without a concentration gradient, some ion exchange may be possible via a charge density effect. Compared to the size of simple atomic cations like K^+, MB^+ is a relatively large molecule with a low charge density. Consequently, the kinetics of MB^+ intercalation into bulk layered materials can be relatively slow or impossible, even with the help of concentration gradients [15]. For example, it has been reported that after pre-expanding the layers with propylamine as an intermediate step, the intercalation of MB^+ into the layered compounds of $KTiNbO_5$ and KNb_3O_8 required two weeks [15,41]. The reported results were ratios of about 0.23 mol per $[TiNbO_5]^-$ and 0.19 mol per $[Nb_3O_8]^-$. In our results presented here, without using pre-expansion, the direct intercalation of MB^+ into $HTiNbO_5$ in water resulted in only a trace amount of intercalation. We found that only 0.056 µmol/g of MB^+ intercalated into $HTiNbO_5$. Given these expectations on typical driving forces involved in intercalation, it was surprising to find that MB^+ intercalated very quickly into HPOX, even from solutions in which the MB^+ concentration was below 50 ppm. It became clear that significant host-guest and guest-guest interactions were involved.

3.1. Electron microscopy

To observe any morphological changes in the new materials, dried samples were examined using scanning electron microscopy (SEM) and transmission electron microscopy (TEM). **Figure 3a** is an SEM image of $HTiNbO_5$. Both $KTiNbO_5$ and $HTiNbO_5$ have dense and layered structures. **Figure 3b** is an SEM image of an air-dried sample of the HPOX material, indicating that it possesses a random, low-density porous structure. This morphology is consistent with a report of a similar restacked material [23]. When air-dried, much of the open porosity in HPOX is lost due to the crushing power of the water-water and the water-oxide intermolecular forces during drying [42]. Although drying of porous materials using supercritical point CO_2 methods can help preserve porosities [38], samples in this work were air-dried at ambient conditions for microscopic analyses and therefore the loss of porosity is expected. In the synthesis

of HPOX, **Figure 3b** shows that the individual $(TiNbO_5^-)_n$ nanosheets aggregated into a continuous solid with the sheets randomly arranged [34].

As described above and elsewhere, this random positioning of the sheets contributes to the porosity of the HPOX material [23,28,38]. The pore walls of the restacked material are composed of just a few restacked sheetsand are therefore only a few nanometers thick [23]. The bright raised lines in **Figure 3b** and **Figure 3c** are due to the formation of wrinkles from the folding and shrinking of the larger sheet-like agglomerates, which are formed during the restacking and drying processes. **Figure 3c** is a typical SEM image of an air-dried sample of the new MB-POX material. It is apparent from the SEM image data that the process of intercalation of MB^+ into the HPOX materials did not cause any remarkable morphological changes to the HPOX.

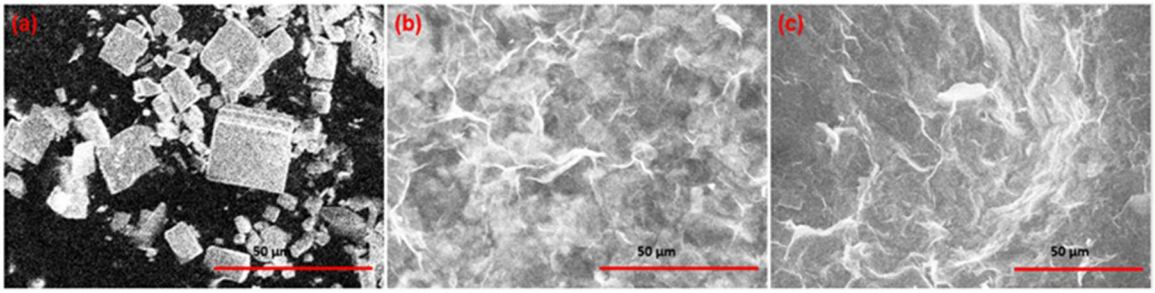

Figure 3. Scanning electron microscopy image of (**a**) $HTiNbO_5$, derived from $KTiNbO_5$, (**b**) the restacked HPOX, and (**c**) MB-POX.

Figure 4a shows a TEM image of the individual $(TiNbO_5^-)_n$ nanosheets found in the colloids, which are derived from the exfoliation of $HTiNbO_5$. **Figure 4a** shows that the $HTiNbO_5$ material was completely exfoliated at pH 9, resulting in a colloid of the individual $(TiNbO_5^-)_n$ nanosheets [35]. The thickness of these nanosheets is approximately 1 nm (0.86 nm) [23], and the lateral dimensions typically range from 0.1 µm to 10 µm, depending on the size of the $HTiNbO_5$ crystallites before exfoliation [43]. **Figure 4b** and **Figure 4c** are TEM images of HPOX and MB-POX material, showing the random order of the restacked $(TiNbO_5^-)_n$ nanosheets [44]. The overlapping, folding, and shrinking of the sheets (during drying) creates wrinkles, which are seen as thin dark lines in the image.

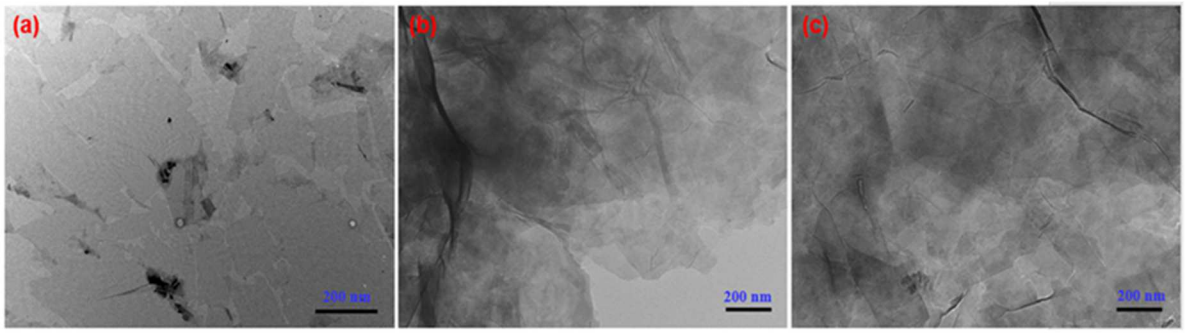

Figure 4. Transmission electron microscopy (TEM) image of (**a**) Exfoliated nanosheet in (TBA)$TiNbO_5$ colloid, (**b**) H^+ restacked porous oxide (HPOX), and (**c**) MB-POX.

3.2. Small-angle X-ray Scattering (SAXS)

The restacked HPOX and the intercalated MB-POX materials were analyzed using small and wide-angle x-ray scattering (SAXS/WAXS) to obtain insights into the nature of the methylene blue (MB^+) intercalation in these materials. All samples were measured in the presence of water to avoid disruption of the structure, especially in the case of HPOX. As determined by SAXS, macroscopically (>100 nm) the HPOX exhibits a change in the mass fractal dimension from $d_m = 2.58$ to $d_m = 2.86$ as it is converted into MB-POX via MB^+ intercalation, indicating a more compact structure in the MB-POX with the presence of MB^+ as compared to the HPOX. HPOX has a local surface

roughness characterized by a Porod exponent of $P_1 = 3.68$, which does not substantially change with MB^+ adsorption, and the two-dimensional nanosheets have a corrugation dimension characterized by a correlation length of 17.8 nm, which increases to 18.1 nm with MB^+ uptake. Evidence that approximately half of the HPOX interlayers undergo intercalation is indicated by the changes to the 2θ peak near 7.5° (see **Figure 5**). HPOX in water results in a broad, disordered interlayer peak corresponding to a d-spacing of 11.83 Å. As compared to $KTiNbO_5$ and $HTiNbO_5$, with d-spacings of 9.2 Å and 8.6 Å respectively, the d-spacing of 11.83 Å for the HPOX in water is strong evidence that the interlayer is well hydrated under these conditions, with the extra water swelling the interlayer regions. In part, the larger d-spacing of HPOX can also be attributed to the turbostratic nature of the restacked nanosheets, which prevents the compact order seen in the parent compounds. After the HPOX is intercalated with MB^+, half of the structure develops a sharper more ordered peak, corresponding to a spacing of 11.04 Å. The intercalation of MB^+ into the HPOX structure to produce MB-POX was observed.

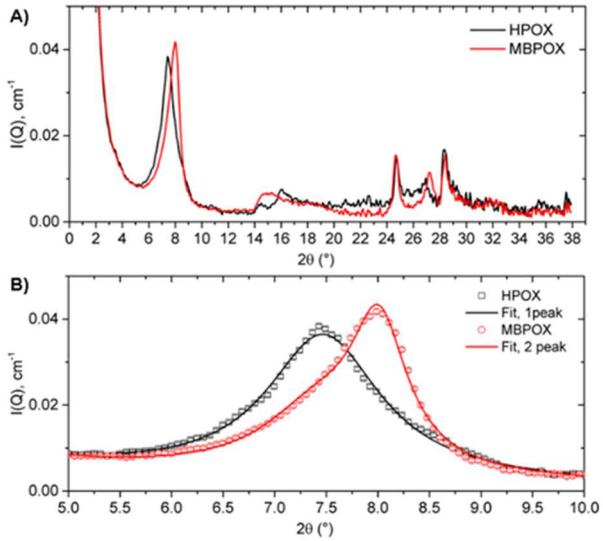

Figure 5. Wide=-angle scattering shows the effect of MB+ adsorption on HPOX in H2O. A) Most features of the HPOX scattering are preserved, yet there is a noticeable shift in the first peak from 2θ ~7.5° to ~8.0°. B) HPOX scattering in water can be fit using a single Lorentzian peak too, however, the MB-exposed HPOX in solution (red) requires two Lorentzians due to partial intercalation of the HPOX layered structure.

The scattering of the HPOX system occurs over 7 decades in intensity in the measured Q-range, demonstrating structure over several orders of magnitude. The signal measured from Q 0.003-0.4 $Å^{-1}$ may be described using a two-level unified power/exponent law. The unified exponential/power-law model developed by Beaucage [45,46] (henceforth referred to as the UEP model), allows extracting information from multiple structural regimes and was fit to I(Q) SAXS curves for each sample. The UEP data fit of HPOX and MB-POX are shown in **Figure 6**. In the UEP model:

$$I(Q) = \sum_{i=0}^{N}\left[G_i\, e^{-Q^2 R_{g,i}^2/3} + \frac{B_i\left(erf\left(QR_{g,i}/\sqrt{6}\right)\right)^{3P_i}}{Q^{P_i}}\right] + \text{bgd} \qquad \textbf{Eq. (2)}$$

Here i = 0 refers to the largest structure to fit with the model, G_i is a constant related to the particle's composition and concentration, R_g is the radius of gyration of the structure, B_i is specific to the type of power-law scattering, and is defined by the regime in which the exponent P_i falls, and bgd is a constant to account for a flat background signal. A scattering exponent $P_i > 4$ corresponds to a diffuse interface. Values of $3 < P_i < 4$ corresponds to surface fractal scattering, where $P_i = 3$ corresponds to rough surfaces, and $P_i = 4$ correspond to smooth surfaces. Values of $2 < P_i < 3$ correspond to mass fractal scattering, where $P_i = 2$ corresponds to an open, loosely connected structure and $P_i = 3$ corresponds to a more highly connected compact structure. $P_i \sim 1$ corresponds to scattering from rod-like objects. The scattering exponent directly gives the fractal dimension, d, as follows: for surface fractals, $d_s = 6\text{-}P_i$ and for mass

fractals, $d_m = P_i$. A two-level UEP model was applied (over the range 0.003-0.4 Å^{-1}) to the H_2O-exposed and MB-exposed HPOX. The first level, i = 0, describes scattering from the macroscopic nanosheets. Although the thickness of the individual nanosheets is on the nanometer length scale, the lateral dimension is in the micrometer range and the total dimension cannot be observed within the SAXS technique's observation window. Thus, R_{g0} was set fixed at 1000 nm, so the only contribution to the i = 0 level is the term $B_0 Q^{-P_0}$. At low-Q, the P_o term due to the large plate-like structures indicates mass fractal scattering with d_m = 2.58, which upon MB^+ adsorption changes to d_m = 2.86, indicating a more compact structure with MB^+ (MB-POX) than without MB^+ (HPOX). The second level, i = 1, describes the size and local surface roughness of the corrugated nanosheets, which form pore spaces of a similar length scale as the nanosheets pack close together. An analysis of the G_2 term in the UEP model, calculation of HPOX and MB-POX scattering length density, and MB^+ outside of the interlayers are available in the supporting information section S1.

The characteristic size is given by an R_{g1} = 17.8 nm for HPOX in water, and this value increases to R_{g1} = 18.1 nm upon MB^+ uptake. The pore surface has a roughness characterized by P_1 = 3.682 ±0.004 which does not substantially change (P_1 = 3.686 ±0.004) with MB^+ uptake.

This is expected since MB^+ uptake is believed to be a physical adsorption process and no chemical reactions take place, which would likely introduce additional inhomogeneities to the surface of the HPOX. Furthermore, to the x-ray probe used here, the physical adsorption of this particular molecule does not appear as a change in roughness because there is very little electron density contrast between MB^+ and water, and the main source of contrast is between HPOX and the MB/H_2O solution. For reference, the signal intensity varies as $I(Q) \sim \Delta\rho^2$, where $\Delta\rho$ is the x-ray scattering length density (which depends on electron density) difference between the two phases under consideration; for MB/H_2O $\Delta\rho^2 \approx 1 * 10^{-12}$Å^{-4} whereas for HPOX/$H_2O$ $\Delta\rho^2 \approx 170 * 10^{-12}$Å^{-4}.

***Exchange in HPOX interlayers*:** The WAXS signal from the HPOX in solution shows a clear shift toward a larger 2θ in the interlayer spacing peak near 7.5° as MB^+ is adsorbed (shown in Fig 5B). A Lorentzian peak with a quadratic baseline

$$I(2\theta) = \sum_i \frac{2A_i}{\pi}\left(\frac{w_i}{4(2\theta - 2\theta_i)^2 + w_i^2}\right) + B(2\theta)^{-2} \qquad \textbf{Eq. (3)}$$

was fit to the data in the 2θ range 4.4-10.7°. A single peak (i = 1) was used for HPOX and two peaks (i = 1, 2) were used for MB-POX. Table 1 presents the fit parameters for the samples. The results indicate that exposure to MB^+ causes partial intercalation of the HPOX interlayers. This is evident by observing that the MB^+ signal is composed of two distinct peaks. One peak (i = 1) has a d-spacing of 11.90 Å, similar to HPOX in water (11.83 Å) and the other (i = 2) has a d-spacing of 11.04 Å. By analyzing and comparing the relative areas of the MB^+ peaks, A_1 and A_2, the fraction of MB-intercalated and the fraction of non-intercalated HPOX in the MB-POX can be obtained.

Table 1. Fit parameters for Lorentzian ??peak for Equation 3, samples are HPOX and MB-POX.

Sample	B	A1	w1	2θ1 (°)	d1 (Å)	A2	w2	2θ2 (°)	d2 (Å)
HPOX	0.16	0.071	1.35	7.47	11.83				
MB-POX	0.18	0.03	1.36	7.43	11.90	0.03	0.66	8.01	11.04

The Lorenztian peak function in Equation 3 above captures the wide-angle lamellar structure and interlayer correlations of the HPOX system. Generally, for a two-phase system, the scattering intensity depends on the concentration of scatterers, *N*, x-ray scattering length density (XSLD) contrast $\Delta\rho$ between the two phases, and a function $F(2\theta)$, which describes the shape and correlations of the system as follows:

$$I(2\theta) = N(\Delta\rho)^2 F(2\theta) \qquad \textbf{Eq. (4)}$$

For the HPOX system, the area of the Lorentzian curve $A = N(\Delta\rho_H)^2 F$, where $\Delta\rho_H = \rho_{HPOX} - \rho_{H2O}$ is the difference in XSLD between HPOX and water. Similarly, if we assume the MB-POX sample contains one fraction

n_H with water and H^+ in the interlayers, and another fraction n_M containing MB, then A_1 and A_2 maybe be expressed as $A_1 = n_H(\Delta\rho_H)^2F$ and $A_2 = n_M(\Delta\rho_{MB})^2F$. Here $\Delta\rho_{MB} = \rho_{HPOX} - \rho_{MB}$ and we treat F as a constant because the major change in the structure of HPOX is whether or not it is intercalated with MB^+. Imposing the normalization condition: $n_H + n_M = 1$, and because $A_1 = A_2$ (see Table 1), we obtain $n_H = n_M * (\Delta\rho_{MB})^2/(\Delta\rho_H)^2$. From this expression, the fraction of the HPOX interlayers containing H_2O is $n_H = 0.54$ and the fraction containing MB^+ is $n_M = 0.46$. Thus, approximately 54 % of the HPOX interlayers, which retain an average d_1 spacing of 11.83-11.90 Å, are believed to not be intercalated with MB^+, while 46 % of the interlayers have a layer spacing of d_2 = 11.04 Å and are believed to be intercalated with MB^+.

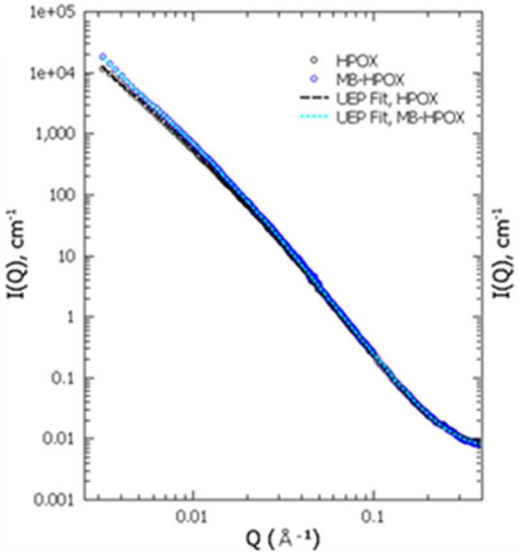

Figure 6. SAXS data of HPOX in water with/without the presence of MB+ (symbols) and fits of the UEP

An x-ray diffraction pattern of dry powdered $KTiNbO_5$ is included in the supporting information (see **Figure S1**). The layer spacing in the stacking direction of $HTiNbO_5$ (acid exchanged $KTiNbO_5$) is 8.5 Å [47]. **Figure 7** shows conventional x-ray diffraction patterns of the dry powdered HPOX and MB-POX materials. The HPOX layer spacing was measured as 11.86 Å, significantly greater than the 8.5 Å found before exfoliating and restacking. Although the restacked HPOX materials were thoroughly dried in the air before x-ray analyses, interlayer hydration is likely the reason for the larger interlayer distance. As discussed later, TGA data (**Figure 11**) suggests that over 10 % of the HPOX mass is due to intercalated and adsorbed water. In addition, restacking of nanosheets randomly orients the sheets as they come together in a turbostratic arrangement. This loss of the in-plane registry between the sheets likely produces corrugation, randomness, and voids that also increase the interlayer spacing, which permits greater hydration of the interlayer.

Upon the aqueous intercalation of MB^+ into HPOX, the interlayer spacing decreased from 11.86 Å for HPOX to 11.07 Å for MB-POX. The presence of the more hydrophobic MB^+ in the interlayers of MB-POX may have driven out interlayer water molecules or allowed it to leave via drying before x-ray analysis, thus decreasing the layer spacing due to the removal of interlayer water. The layer spacing in MB-POX due to the MB^+ is discussed later.

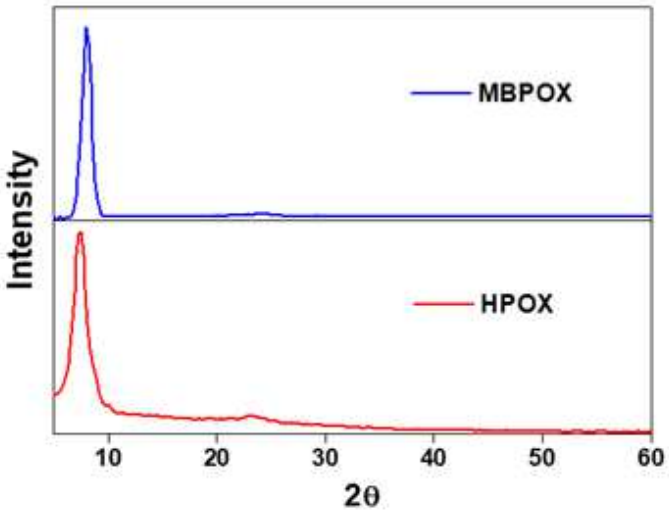

Figure 7. X-ray diffraction patterns of dry HPOX and MB-POX. The single peaks found are at 7.45º and 7.98º 2θ, for HPOX and MB-POX, respectively.

3.3. Quantitative analysis of the MB^+ dye content in MB-POX

During the MB^+ intercalation processes, after about 10 minutes of titrating with the 50 ppm MB^+ solution, the fast disappearance of the MB^+ in the supernatant was no longer occurring and the solid MB-POX was close to saturated. To promote the complete intercalation of MB^+ into the HPOX materials (under dilute conditions) the as-titrated MB-POX materials were then left in 2.5 ppm MB^+ for 12 h. After removing the supernatant, the quantity of MB^+ dye that was bound inside of the MB-POX was measured by using the supernatant MB^+ concentration and the total amount of MB^+ that was added during the intercalation process. However, because the MB-POX materials were rinsed thoroughly to remove any non-specifically bound MB^+, the water from all the rinses was also analyzed to quantify any removed MB^+. Quantification of MB^+ in solution was done via its absorbance at 664 nm using UV-Vis absorption spectroscopy. The well-rinsed MB-POX solids were found to contain 226 mg of MB^+ per gram of HPOX, with a relative error of ±5%. This is equivalent to 795 µmol/g ±5%.

Quantification of the MB^+ content in MB-POX was also analyzed using energy-dispersive x-ray spectroscopy (EDX) on dried samples of MB-POX. The molecular formula for MB^+ is $C_{16}H_{18}N_3S$, it was therefore assumed that quantification of S in MB-POX directly correlated with the MB^+ content. Considering only Ti, Nb, and S, EDX results indicated that the relative atomic amounts of each found in MB-POX were 43.628 %, 39.823 %, and 16.549 %, respectively (see **Figure S3**). Though the Ti-Nb ratio is expected to be 1, EDX found the ratio to be 0.91 in MB-POX. However, this is a common occurrence for this material, when it is analyzed via EDX [48]. By taking the average of the relative ratios, S to Ti and S to Nb, the empirical formula of MB-POX via EDX was determined to be $(MB)_{0.397}H_{0.603}TiNbO_5$. Quantification via EDX yielded the same result as was obtained by UV-Vis spectroscopy, $(MB)_{0.4}H_{0.6}TiNbO_5$ (see discussion above).

To put the MB^+ content results into perspective, the following calculations were performed. Assuming the ideal electrostatics-based formula of MB-POX to be $(MB)_xTiNbO_5$, where x = 1, the theoretical maximum amount of MB^+ that can be incorporated by the HPOX was calculated to be 563 mg/g, which is equivalent to 1979.5 µmol/g. Comparing the experimental result to the theoretical value, x = (226 mg/g)/(563 mg/g), we find that x = 0.401. While from the literature result, a molar ratio of 0.30 was found for the similar layered oxide-MB composite [49]. On the bases of charge, this current study implies that 40 % of the theoretical maximum amount of MB^+ was intercalated by the HPOX. If x = 0.40 in $[MB]_x(TiNbO_5)$, the remaining charge balance (1-x) is equal to 0.60, which represents a monovalent cation capacity that is being satisfied by other cations within the solid. Considering the syntheses of

HPOX and MB-POX, the only other cation possibilities are K^+, H^+, and TBA^+. The acid exchange process of the parent $KTiNbO_5$ was done extensively, so all K^+ should have been removed. Any K^+ present would prevent nanosheet exfoliation and those unexfoliated chunks of impurities would have been removed during the synthesis. The restacking of the colloidal sheets was done with strong acid, followed by extensive rinsing with water, so only traces of TBA^+, if any at all, would have been present in the HPOX material. Therefore, H^+ is the most likely cation that is supplying the balance of cationic charge in the MB-POX. As a result, the compound formula of the new MB-POX composite is believed to be $(MB)_{0.4}H_{0.6}TiNbO_5$.

A result of $(MB)_{0.4}H_{0.6}TiNbO_5$ for MB-POX may appear to imply incomplete intercalation, however, the difference in size between the H^+ and MB^+ cations could help explain why reaching a theoretical maximum loading of 100% may not be possible. Given that MB^+ occupies a much larger volume than H^+ or K^+, the intercalated MB^+ molecules may not pack close enough to each other to satisfy the charge density of the metal oxide layers. The individual restacked metal oxide sheets are two-dimensional (2-D), and the layers of cations have a 2-D interaction with the sheets. Therefore, to gain insight a comparison is needed between the 2-D charge density of an MB+ molecule and the 2-D charge density of an anionic $(TiNbO_5^-)_n$ nanosheet [23]. According to a literature report by Hähner, the dimensions of an MB+ molecule are 1.69 nm x 0.74 nm x 0.38 nm [50,51]. As they come together, there are several orientations that MB^+ molecules can adopt with respect to the sheets. Three packing arrangements of intercalated MB^+ in the solid are depicted in **Figure 8**. **Figure 8a** shows MB^+ standing upright yet tilted. **Figure 8b** shows a three-layer stack of MB^+ molecules, lying down parallel to the sheet layers. **Figure 8c** shows packed MB^+ molecules standing vertical with their long axes perpendicular to the surface of the sheets. The x-ray data and charge density analysis that follows implies that only the arrangement depicted in **Figure 8a** adequately accounts for the observed data obtained for MB-POX. The high loading of MB^+ found in MB-POX suggests that dimerization and higher aggregation of the MB^+ are probable. This implies that the MB^+ molecules must be very close to each other, to enable a higher packing density. The UV-Vis absorption data above shows a peak shift for MB^+ and this corroborates the existence of dye-dye interactions. Dye-dye interactions and their spectroscopic signatures have been observed by others when MB^+ is intercalated into layered materials [14,41,49].

A charge density analysis requires the use of the 2-D footprint of the MB^+ molecule as it interacts in its various orientations with the surface of a 2-D sheet. The 2-D charge densities of the metal oxide sheet and the MB^+ molecules are also utilized; however, it is convenient to take the inverse of the charge densities to obtain the *square area per charge ratios*. A previous study has reported a surface area per charge ratio of a single $(TiNbO_5^-)_n$ sheet as 0.123 nm^2/charge [52]. In the upright perpendicular orientation of the MB^+ regarding the sheets, with MB^+ standing vertical on the end of the long axis (see **Figure 8c**), each MB^+ would require a footprint (surface area) of 0.281 nm^2. Therefore, for this orientation, the inverse two-dimensional charge density of the singly charged MB^+ is 0.281 nm^2/charge. For this same vertical orientation, a comparison of the value of the *square area per charge ratio* of the sheet to that of the MB^+ finds that the MB^+ requires 2.286 times more square area per charge than the sheet offers. In other words, for this orientation, the maximum loading capacity of the HPOX for MB^+ is, (0.123 nm^2/charge) / (0.281 nm^2/charge), or 43.74%. Relative to the electrostatic theoretical maximum of 100 %, 43.74% is close to the experimentally measured value of 40% found in the new MB-POX material. Likewise, for a flat horizontal orientation of MB^+ in between the sheets, using a footprint of 1.69 nm x 0.74 nm, a ratio of 1.25 nm^2/charge is calculated. For this horizontal orientation, the MB^+ requires 10.17 times more square area per charge than the sheet offers, and this translates into a potential loading of about 9.8 %, relative to the theoretical maximum based on electrostatics. These calculations imply that the footprints of MB^+ in either orientation described do not permit MB^+ to fully charge to compensate for the anionic charge on the $(TiNbO_5^-)_n$ sheets, thus resulting in apparently partial intercalations that in fact may be complete. Therefore, it is likely that the balance of the positive charge in MB-POX is supplied by H^+ (or H_3O^+) and that a formulation of $(MB)_{0.4}H_{0.6}TiNbO_5$ is reasonable.

X-ray data shows that for MB-POX the interlayer spacing is 1.104 A. A compound structure with a single layer of MB^+ laying down flat in between the layers does not fit the x-ray data. Possibly, the MB^+ molecules are stacked on top of each other horizontally in triple stacks in between the oxide sheets (see **Figure 8b**). This would result in an MB+ loading of 29.5%. As the vertical perpendicular orientation described above produces a higher loading of 43.74%, it is considered to be more likely, as it more closely aligns with the quantitative analysis data obtained. Also,

if the MB^+ were lying down horizontally in stacks of three, the expected layer spacing would be d = 1.14 nm. The x-ray data on MB-POX show that the d-spacing between the layers of sheets is 1.104 nm, and the triple stacking of MB^+ does not match the x-ray data. However, if the MB^+ are standing vertical and on-end (**Figure 8c**) as described earlier in the charge density discussion, the expected d-spacing would be around 1.69 nm, which also does not fit the x-ray data of 1.104 nm. If the vertical on end MB^+ molecules were tilted at an angle of 40.4° up from the plane of the sheets (see **Figure 8a**), then the d-spacing of the layers of metal oxide would agree with the x-ray data and be equal to 1.104 nm [22]. Tilted MB^+ orientations at similar angles have been reported by others. J. Ma et al. reported that the interlayer spacing for single layer MB incorporated into calcium niobate nanosheets was 1.22 nm, and the tilt angle was 46° from the normal to the layer (44° up from the plane of the layer) [30]. Therefore the configuration in **Figure 8a** with the MB^+ titled is a reasonable conclusion, which fits the observed data.

Incorporating dyes onto metal oxides has potential utility in a variety of applications, including the use of dyes as photosensitizers. To provide additional perspective and for easier comparison to the literature, in the following theoretical calculation, we have treated the observed MB^+ loading as if all the MB^+ were exclusively surface adsorbed with none present as intercalated between nanosheets. This theoretical calculation also highlights the ability of HPOX to uptake large amounts of MB^+. Using the dimensions of MB^+ as above, this approach assumes that MB^+ is surface adsorbed, lying flat with its broadside on the surface, the footprint of this horizontal orientation of an individual MB^+ molecule is estimated to be 1.251 nm^2. Assuming that the porous material's available surface area can be completely covered by a monolayer of MB^+ molecules, the maximum number of molecules that can be surface-adsorbed is equal to the total available surface area of the material divided by the footprint area of an MB^+ molecule. Here we have used an HPOX surface area of 150 m^2/g, which is an estimate based on previous reports of the same material from our lab using supercritical point CO_2 drying [38]. However, the HPOX and the MB-POX samples synthesized in this study were never dried, so a surface area of 150 m^2/g is an estimate. Using these numbers and the orientation stated, the theoretical maximum surface-only adsorption of MB^+ is calculated to be 199.17 µmol/g. As presented above, the analysis of the content of MB^+ in MB-POX was found to be 794.65 µmol/g. If 794.65 µmol/g were surface-only adsorbed, then the surface coverage efficiency would be (794.65 µmol/g) / (199.17 µmol/g), or about 399 %. Even though HPOX has a reasonably high external surface area, the internal area in between the layered overlapping sheets is greater than the external surface area.

To show the general applicability and relative effectiveness of this new synthetic process, a different layered metal oxide, potassium hexaniobite, $K_4Nb_6O_{17}$, was modified similarly and the product was also used to intercalate MB^+. $K_4Nb_6O_{17}$ was transformed into a porous material using the same synthetic methods used for the $KTiNbO_5$ material to make HPOX. The analogous porous oxide via $K_4Nb_6O_{17}$ is referred to as HexaPOX, and they were synthesized by restacking $(Nb_6O_{17}^{4-})_n$ nanosheet colloids with acid. The experimental details for HexaPOX are described in the supporting information section (S2). Like HPOX, this new HexaPOX material has an open-pore structure and improved surface area. HexaPOX was also used as a host for the intercalation of MB^+ dissolved in water. The intercalation of MB^+ titrated into the HexaPOX material was completed within minutes and much like what occurred with the MB^+ intercalation into HPOX. The result was a deep, blue-colored solid, referred to as MB-HexaPOX. The well-rinsed MB-Hexa-POX solids were found to contain 178 mg of MB^+ per gram of Hexa-POX, with a relative error of ±5%. This is equivalent to 627 µmol/g ±5%. For comparison, the MB-POX materials contained 226 mg of MB^+ per gram of HexaPOX.

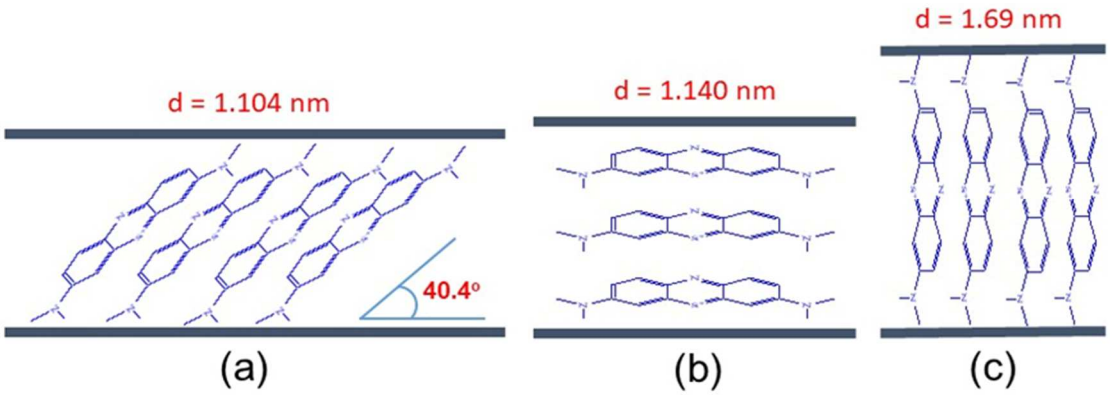

Figure 8. Possible arrangements of the MB^+ molecules inside MB-POX and the interlayer spacing that would result: a) tilted, b) horizontal, and c) vertical.

3.4. UV-Vis and Raman spectroscopy

Figure 9a shows a UV-Vis transmission absorption spectrum of a methylene blue (methylthioninium chloride) solution in water. The absorption maximum of the MB^+ monomer in water appears at 664 nm [36]. In water, the naturally occurring dimer of MB^+, $(MB^+)_2$, exhibits an absorption peak at 605 nm [36]. As the two cationic MB^+ molecules associate into a dimer, the positive charge on the sulfur atom in each MB^+ molecule likely interacts favorably with the π electrons of the opposite MB^+ molecule, thus altering the energy of the π electrons, resulting in a blue shift the π to π* electronic transition. This is seen as the dimer absorption band in the red region at 605 nm. The lone pair electrons on the central nitrogen may also be a factor in the dimerization. Figure 9b shows a UV-Vis diffuse reflectance (UV-Vis-DRS) absorption spectrum of an air-dried film of the MB-POX material. The MB-POX spectrum shows two peaks. One peak is at 601 nm, which appears to correspond to the closely interacting MB^+ molecules (possibly as dimers or higher aggregates), and a second peak is at 686 nm corresponding to the monomers. Compared to the $(MB^+)_2$ dimer in solution, the peak at 601 nm in MB-POX is blue-shifted by 4 nm, which may be due to the presence of higher-order MB^+ aggregates. The possibility of more than two MB^+ molecules interacting is consistent with the previously discussed results. As has been shown above, the MB-POX exhibited a very high loading of MB^+, therefore it is likely that many of the MB^+ molecules are close to each other in the solid, packing as dimers, trimers, or higher aggregates. Furthermore, the SAXS data suggests that there are large regions in the MB-POX material, where the intercalated MB^+ fills the interlayer regions.

The MB-POX also exhibits a UV-Vis-DRS absorption peak at 686 nm (**Figure 9b**). Although the peak is red-shifted by about 22 nm as compared to MB^+ in solution, this absorption peak is likely due to the MB^+ monomers within the solid. The reason for the redshift in this peak could be explained by the interaction of the cationic monomers with the negatively charged $(TiNbO_5^-)_n$ nanosheets. The anionic nanosheets may contribute some electron density to the MB^+. Such a sheet-monomer interaction would lower the energy of the MB π - π* transition, thus causing a red shift in the absorption peak. According to literature, the doubly protonated methylene blue absorbs light at around 775 nm [40]. The absence of this peak in the present UV-Vis data further supports the conclusion made above that the protons (H^+) inside the MB-POX were probably co-intercalated with MB^+ rather than being bonded directly to the MB^+ molecule.

Raman spectra of the HPOX and MB-POX materials are shown in **Figure 9**. HPOX is composed of restacked nanosheets, which are in random orientations. The nanosheets are chemically identical to the metal oxide layers in the parent material, $KTiNbO_5$. Instead of K^+, HPOX has H^+ sandwiched between the restacked nanosheets [23]. The $(TiNbO_5^-)_n$ nanosheets are composed of edge shared and corner shared TiO_6 and NbO_6 octahedra. Based on previous Raman spectroscopic studies done on $KTiNbO_5$ [53,54], the following peak assignments were made for the as-prepared HPOX and MB-POX materials.

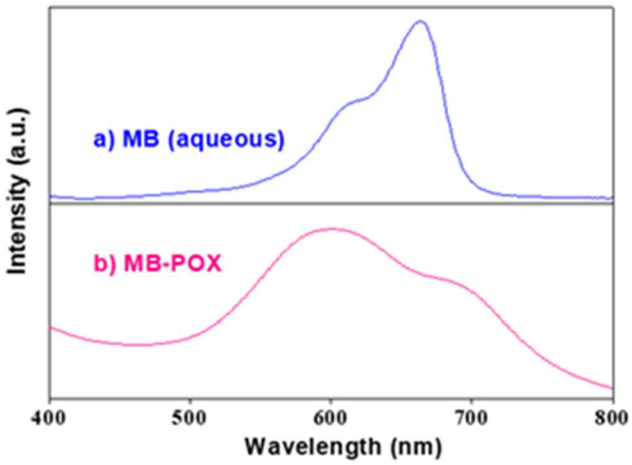

Figure 9. UV-Vis spectrum of (a) aqueous methylene blue chloride and (b) the UV-Vis-DRS spectrum of MB-POX (sample was a film dried in the air).

The HPOX spectrum also exhibits the three characteristic bands found in $KTiNbO_5$. For $KTiNbO_5$, they are 543.8 cm^{-1} (Ti-O-Ti), 656.4 cm^{-1} (Nb-O-Nb), and 891.7 cm^{-1} (Nb=O) [53]. In the HPOX spectrum shown (**Figure 10b**), these bands correspond to the 537 cm^{-1}, 661 cm^{-1}, and 882 cm^{-1} band, respectively. The nature of the interlayer ions in layered transition metal oxide materials has been shown to modify Raman spectroscopic features. Therefore, the shifts in the spectral peak positions of the three characteristic bands found in $KTiNbO_5$ vs. HPOX are expected [55]. For the MB-POX material, the corresponding bands appear to be at 480 cm^{-1}, 679 cm^{-1}, and 906 cm^{-1}. The MB-POX band at 480 cm^{-1} (Ti-O-Ti) exhibits a large shift of 57 cm^{-1}. The presence of the MB^+ in the interlayer may also produce distortions in the TiO_6 octahedra and the planarity of the restacked nanosheets [54]. After the intercalation of MB^+, the terminal Nb=O bond vibration shifted from 891.7 to 906 cm^{-1}. This shift may have resulted from the loss of the H^+ interaction with Nb=O, replaced now with the interaction of interlayer MB^+ with the negatively charged oxygen on the Nb=O. In addition, the FTIR spectrum of the MB-POX was found to be consistent with the Raman data (see SI **Figure S2**).

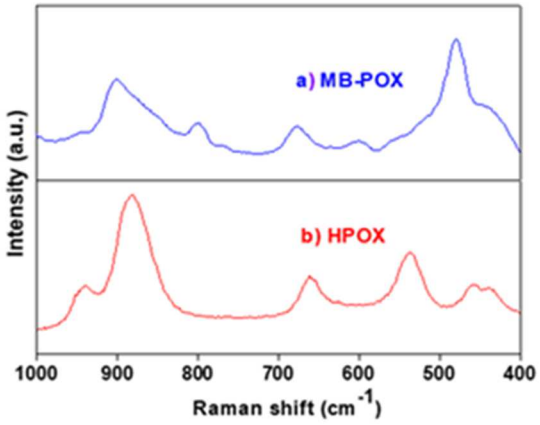

Figure 10. Raman spectra of (a) MB-POX and (b) HPOX.

3.5. Thermogravimetric analysis

Shown in **Figure 11** are thermogravimetric (TGA) analyses performed for the HPOX material and MB-POX. In both cases, the temperature range scanned was 25-1000 °C. In the HPOX, the mass loss from 25-200 °C was ascribed to the evaporation of surface-bound and internally trapped water. The mass loss above 200 °C was attributed to a topotactic dehydration reaction that can occur in the interlayer of this material at elevated temperatures [56]. HPOX

is essentially similar to the unexfoliated $HTiNbO_5$, however, HPOX has a porous structure. The following reaction summarizes the topotactic dehydration reaction that transforms $HTiNbO_5$ into $Ti_2Nb_2O_9$.

$$2\ HTiNbO_5 \rightarrow Ti_2Nb_2O_9 + H_2O$$

In the MB-POX material, the mass loss from 25 to 150 °C is also attributed to the evaporation of surface and internally trapped water. The mass loss above 300 shows some topotactic dehydration and the decomposition of organic material in the intercalated MB^+ dye. Much of the mass loss occurred above 150 °C and continued up to 973 °C. The total mass loss in MB-POX was about 12 % and the rate of the loss appears to be more gradual than other MB^+ intercalated materials reported in the literature, indicating that the MB^+ inside MB-POX appears to be stabilized by this host's layered oxide environment.

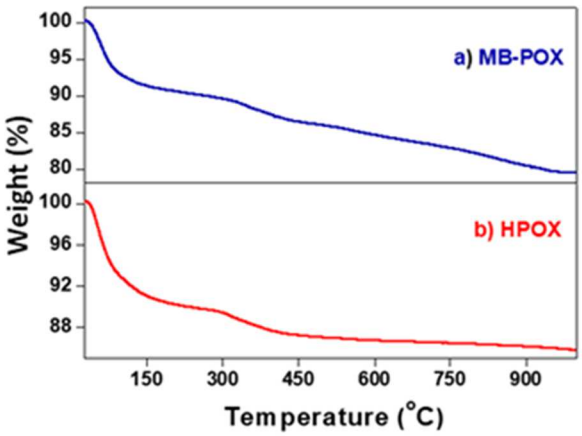

Figure 11. Thermogravimetric analysis (TGA) curves for (a) MB-POX and (b) HPOX.

4. Conclusion

The acidic porous oxide, HPOX, was successfully synthesized by the acid restacking colloidal nanosheets, derived from exfoliated $KTiNBO_5$. The HPOX solids were used as a host to successfully intercalate methylene blue (MB^+) in water. HPOX demonstrated a high affinity for MB^+, intercalating 226 mg/g (= mg MB^+/g of HPOX, or 794.65 µmol/g) from dilute solutions within minutes to yield a unique MB^+ loaded porous oxide, MB-POX. Quantitative analyses, x-ray diffraction, small- and wide-angle x-ray scattering (SAXS/WAXS), Raman spectroscopy, FTIR, and UV-Vis-DRS and TGA data for the MB-POX material corroborate that MB^+ was intercalated in between the restacked layers of $(TiNbO_5^-)_n$ nanosheets in the HPOX host. For a large fraction of MB-POX, the predominant arrangement of the intercalated MB^+ was with MB^+ packed together in aggregates, standing upright on their long axes, yet tilted at 40.4° up from the plane of the restacked nanosheets. The balance of the MB-POX solid is likely intercalated with a mixture of H^+, MB^+ monomers, and MB^+ dimers.

Compared to a theoretical maximum based on electrostatic parameters, quantitative analyses indicated that the cations in MB-POX were 40 % MB^+ and 60 % H^+, which led to an MB-POX empirical formula of $(MB)_{0.4}H_{0.6}TiNbO_5$. Structural analyses using small angle x-ray scattering (SAXS) indicate that the interlayer spaces of MB-POX were composed of two phases, one with predominantly MB^+ corresponding to 46 % of the total interlayer volume, and a second phase consistent with an interlayer composition of hydrated H^+ and possibly monomeric MB^+ corresponding to 54 % of the total interlayer volume. All SAXS measurements were performed in water, which led to the hydration of the interlayer regions of HPOX and of the MB-POX regions where H^+ was located. The facile hydration of HPOX and its open pore structure may enhance the intercalation kinetics of this material by producing pre-expanded interlayer spaces and improved mass transport within the solid for a subsequent ion exchange. This is the first report of a methylene blue metal oxide composite synthesis that uses an acid-restacked layered metal oxide material as the initial host for a subsequent intercalation of MB^+. The synthetic strategy explored here ,in general, can be applied to create similar composites with other layered oxide materials and dyes, which may be useful in the study of electron transfer mediation, sensors, redox indicators, pigment stabilization, photocatalysis, and energy conversion.

Supporting information

A supporting information file is available, containing the following. **S1**- Analysis of the G_2 term in the UEP model, calculation of HPOX and MB-POX scattering length density, and MB^+ outside the interlayers analysis**. S2-** Synthesis of acid restacked HexaPOX from potassium hexanoate. **Figure S1-** X-ray diffraction pattern of powdered $KTiNbO_5$. **Figure S2-** Fourier transforms the infrared spectrum of (a) crystalline methylthioninium chloride (methylene blue chloride), (b) MB-POX, and (c) the HPOX host before intercalation. **Figure S3-** EDX analysis of MB-$TiNbO_5$ (MB-POX) composite.

Authors' contributions

All authors contributed to data analysis, drafting and revising of the paper and agreed to be responsible for all the aspects of this work.

Acknowledgments

The authors would like to thank Dr. Mahesh Narayan and his group for sharing their centrifuge. Special Thanks to Dr. Jorge Gardea-Torresdey for his generous instructions and guidance. TEM instrumentation was provided by New Mexico State University and the National Science Foundation under MRI-DBI-0520956. small-angle x-ray scattering measurements were performed at the University of Texas at El Paso's Department of Physics.

Declaration of competing interest

The authors declare no competing interest.

Funding

This paper received no external funding.

Data availability

Data will be made available on request.

References

[1] M.T.Yagub, T.K. Sen, S. Afroze, H.M. Ang, Dye and its removal from aqueous solution by adsorption: A review. Adv. Colloid Interface Sci. 209 (2014) 172-184.
[2] P. Bradder, SK. Ling, S. Wang, S. Liu, Dye adsorption on layered graphite oxide, J. Chem. Eng. Data. 56 (2010) 138-141.
[3] J. Bujdák, Effect of the layer charge of clay minerals on optical properties of organic dyes: A review. Appl. Clay Sci. 34 (2006) 58-73.
[4] FJ. Quites, C. Bisio, GV. Rita de Cássia, R. Landers, L. Marchese, HO. Pastore, Vanadium oxide intercalated with polyelectrolytes: Novel layered hybrids with anion exchange properties, J. Colloid Interface Sci. 368 (2012) 462-469.
[5] M. Laipan, L. Xiang, J. Yu, BR. Martin, R. Zhu, J. Zhu, H. He, A. Clearfield, L. Sun, Layered intercalation compounds: Mechanisms, new methodologies, and advanced applications, Prog. Mater. Sci. 109 (2020) 100631.
[6] AA. Martí, JL. Colón, Photophysical characterization of the interactions among tris(2,2′-bipyridyl)ruthenium(ii) complexes ion-exchanged within zirconium phosphate, Inorg. Chem. 49 (2010) 7298.
[7] R. Uppuluri, AS. Gupta, AS. Rosas, TE. Mallouk, Soft chemistry of ion-exchangeable layered metal oxides, Chem. Soc. Rev. 47 (2018) 2401-2430.
[8] NC. Dafader, T. Akter, ME. Haque, SP. Swapna, S. Islam, D. Huq, Effect of acrylic acid on the properties of polyvinylpyrrolidone hydrogel prepared by the application of gamma radiation, Afr. J. Biotechnol. 11 (2012) 13049-13057.
[9] M. Wainwright, DA. Phoenix, L. Rice, SM. Burrow, J. Waring, Increased cytotoxicity and phototoxicity in the methylene blue series via chromophore methylation, J. Photochem. Photobiol. B, Biol. 40 (1997) 233-239.
[10] J. Pan, L. Wang, G. Zhang, D. Gong, Intercalation of 2-butyl-4-methylphenol to g–c rich region of DNAand the role of hydroxypropyl-β-cyclodextrin, J. Photochem. Photobiol. B, Biol. 151 (2015) 125-134.
[11] NP. Mohabansi, VB. Patil, N. Yenkie, A comparative study on photodegradation of methylene blue dye effluent by advanced oxidation process by using tio2/zno photo catalyst, Rasayan J. Chem. 4 (2011) 814-819.
[12] SO. Kelley, JK. Barton, NM. Jackson, MG. Hill, Electrochemistry of methylene blue bound to a DNA-modified electrode, Bioconjug. Chem. 8 (1997) 31-37.

[13] J. Zhang, Y. Zheng, G. Jiang, C. Yang, M. Oyama, Electrocatalytic evaluation of liquid phase deposited methylene blue/tio2 hybrid films, Electrochem. commun. 10 (2008) 1038-1040.
[14] X. Zhang, D. Li, F. Yin, J. Gong, X. Yang, Z. Tong, X. Xu, Characterization of a layered methylene blue/vanadium oxide nanocomposite and its application in a reagentless H_2O_2 biosensor, Appl. Biochem. Biotechnol. 172 (2014) 176-187.
[15] S. Wang, C. Liu, L. Liu, X. Zhang, J. Gong, Z. Tong, Preparation and electrochemical behavior of methylene blue intercalated into layered triniobate potassium, Inorg. Nano-Met. Chem. 42 (2012) 251-255.
[16] M. Rafatullah, O. Sulaiman, R. Hashim, A. Ahmad, Adsorption of methylene blue on low-cost adsorbents: A review. J. Hazard. Mater. 177 (2010) 70-80.
[17] T. Liu, Y. Li, Q. Du, J. Sun, Y. Jiao, G. Yang, Z. Wang, Y. Xia, W. Zhang, K. Wang, Adsorption of methylene blue from aqueous solution by graphene, Colloids Surf., B. 90 (2012) 197-203.
[18] YC. Sharma, Optimization of parameters for adsorption of methylene blue on a low-cost activated carbon, J. Chem. Eng. Data. 55 (2009) 435-439.
[19] S. Ahmed, Z. Ahmad, A. Kumar, M. Rafiq, VK. Vashistha, MN. Ashiq, A. Kumar, Effective removal of methylene blue using nanoscale manganese oxide rods and spheres derived from different precursors of manganese, J. Phys. Chem. 155 (2021) 110121.
[20] J. Cenens, R. Schoonheydt, Visible spectroscopy of methylene blue on hectorite, laponite b, and barasym in aqueous suspension, Clays Clay Miner. 36 (1988) 214-224.
[21] MD. Richards, CG. Pope, Adsorption of methylene blue from aqueous solutions by amorphous aluminosilicate gels and zeolitex, J. Chem. Soc., Faraday. 92 (1996) 317-323.
[22] U. Unal, Y. Matsumoto, N. Tamoto, M. Koinuma, M. Machida, K. Izawa, Visible light photoelectrochemical activity of k4nb6o17 intercalated with photoactive complexes by electrostatic self-assembly deposition, J. Solid State Chem. 179 (2006) 33.
[23] T. Akter, GB. Saupe, Exceptional sensitizer dye loading via a new porous titanium–niobium metal oxide with tris(2,2′-bipyridyl)ruthenium(ii) in the structure, ACS Appl. Nano Mater. 1(2018) 5620-5630.
[24] S. Masud, M. Zarei, ML. Lopez, Gardea-Torresdey J, Ramana CV, Saupe GB, Photoreduction of metallic co-catalysts onto novel semiconducting metal oxides, Mater Sci Eng, B. 174 (2010) 66.
[25] K. Maeda, TE. Mallouk, Comparison of two-and three-layer restacked dion–jacobson phase niobate nanosheets as catalysts for photochemical hydrogen evolution, J. Mater. Chem. 19 (2009) 4813-4818.
[26] H. Hata, Y. Kobayashi, V. Bojan, WJ. Youngblood, TE. Mallouk, Direct deposition of trivalent rhodium hydroxide nanoparticles onto a semiconducting layered calcium niobate for photocatalytic hydrogen evolution, Nano Lett. 8 (2008) 794-799.
[27] U. Unal, Y. Matsumoto, N. Tanaka, Y. Kimura, N. Tamoto, Electrostatic self-assembly deposition of titanate (iv) layered oxides intercalated with transition metal complexes and their electrochemical properties, J. Phys. Chem. B. 107 (2003) 12680.
[28] GB. Saupe, Y. Zhao, J. Bang, NR. Yesu, GA. Carballo, R. Ordonez, T. Bubphamala, Evaluation of a new porous titanium-niobium mixed oxide for photocatalytic water decontamination, Microchem J. 81 (2005) 156.
[29] R. Ma, T. Sasaki, Two-dimensional oxide and hydroxide nanosheets: Controllable high-quality exfoliation, molecular assembly, and exploration of functionality, Acc. Chem. Res. 48 (2014) 136-143.
[30] J. Ma, Z. Zhang, M. Yang, Y. Wu, X. Feng, L. Liu, X. Zhang, Z. Tong, Intercalated methylene blue between calcium niobate nanosheets by esd technique for electrocatalytic oxidation of ascorbic acid, Microporous Mesoporous Mater. 221 (2016) 123-127.
[31] H. Rebbah, G. Desgardin, B. Raveau, Les oxydes atimo5: Echangeurs cationiques, Mater. Res. Bull. 14 (1979) 1125.
[32] F. Zhang, J. Ilavsky, GG. Long, JPG. Quintana, AJ. Allen, PR. Jemian, Glassy carbon as an absolute intensity calibration standard for small-angle scattering, Metall. Mater. Trans. A: Phys. 41 (2010) 1151-1158.
[33] H. Rebbah, G. Desgardin, B. Raveau, Nonstoichiometric oxides with a layer structure: The compounds a1−x(ti1−xm1+x)o5, J. Solid State Chem. 31 (1980) 321-328.
[34] H. Wang, S. Wu, T. Cao, B. Zhao, J. Ruan, J. Cao, Z. Tong, X. Zhang, Self-assembly behavior of layered titanium niobate and methylene blue cation and electrochemical detection of dopamine, Mater. Res. (2021) 1-10.
[35] GH. Du, Y. Yu, Q. Chen, RH. Wang, W. Zhou, LM. Peng, Exfoliating ktinbo5 particles into nanosheets, Chem. Phys. Lett. 377 (2003) 445-448.
[36] M. Fang, CH. Kim, TE. Mallouk, Dielectric properties of the lamellar niobates and titanoniobates am2nb3o10 and atinbo5 (a = h, k, m = ca, pb), and their condensation products ca4nb6o19 and ti2nb2o9, J. Mater. Chem. 11(1999) 1519-1525.
[37] R. Abe, K. Shinohara, A. Tanaka, M. Hara, JN. Kondo, K. Domen, Preparation of porous niobium oxides by soft-chemical process and their photocatalytic activity, J. Mater. Chem. 9 (1997) 2179.
[38] S. Masud, M. Zarei, ML. Lopez, J. Gardea-Torresdey, CV. Ramana, GB. Saupe, Photoreduction of metallic co-catalysts onto novel semiconducting metal oxides, J. mater. sci. eng., B. 174 (2010) 66-70.
[39] Y. Wang, H. Arandiyan, J. Scott, A. Bagheri, H. Dai, R. Amal, Recent advances in ordered meso/macroporous metal oxides for heterogeneous catalysis: A review, J. Mater. Chem. 5 (2017) 8825-8846.
[40] J. Bujdák, M. Janek, J. Madejová, P. Komadel, Influence of the layer charge density of smectites on the interaction with methylene blue, J. Chem. Soc., Faraday trans. 94 (1998) 3487.
[41] X. Zhang, C. Liu, L. Liu, D. Zhang, T. Zhang, X. Xu, Z. Tong, Intercalation of methylene blue into layered potassium titanoniobate ktinbo5: Characterization and electrochemical investigation, J. Mater. Sci. 45 (2010) 1604-1609.

[42] T. Heinrich, U. Klett, J. Fricke, Aerogels—nanoporous materials part i: Sol-gel process and drying of gels, J. Porous Mater. 1 (1995) 7-17.
[43] R. Ma, T. Sasaki, Nanosheets of oxides and hydroxides: Ultimate 2d charge-bearing functional crystallites, Adv. Mater. 22 (2010) 5082-5104.
[44] S. Dong, N. Lv, Y. Wu, G. Zhu, X. Dong, Lithium-ion and sodium-ion hybrid capacitors: From insertion-type materials design to devices construction, Adv. Funct. Mater. 31 (2021) 2100455.
[45] G. Beaucage, Approximations leading to a unified exponential/power-law approach to small-angle scattering, J. Appl. Crystallogr. 28 (1995) 717-728.
[46] G. Beaucage, Small-angle scattering from polymeric mass fractals of arbitrary mass-fractal dimension, J. Appl. Crystallogr. 29 (1996) 134-146.
[47] T. Nakato, H. Miyata, K. Kuroda, C. Kato, Synthesis of methylviologen-htinbo5 intercalation compound and its photochemical behavior, J Phys Chem Solids. 6 (1988) 231-238.
[48] J. Li, X. Zhang, B. Pan, J. Xu, L. Liu, J. Ma, M. Yang, Z. Zhang, Z. Tong, Application of a nanostructured composite material constructed by self-assembly of titanoniobate nanosheets and cobalt porphyrin to electrocatalytic reduction of oxygen, Chin. J. Chem. 34 (2016) 1021-1026.
[49] W. Qu, F. Chen, B. Zhao, J. Zhang, Preparation and visible light photocatalytic performance of methylene blue intercalated k4nb6o17, J. Phys. Chem. Solids. 71 (2010) 35-41.
[50] TH. Pham, GW. Brindley, Methylene blue adsorption by clay minerals. Determination of surface areas and cation exchange capacities, Clays Clay Miner. 18 (1970) 203-212.
[51] G. Hähner, A. Marti, ND. Spencer, WR. Caseri, Orientation and electronic structure of methylene blue on mica: A near edge x-ray absorption fine structure spectroscopy study, J. Chem. Phys. 104 (1996) 7749-7757.
[52] J. Ma, J. Wu, J. Zheng, L. Liu, D. Zhang, X. Xu, X. Yang, Z. Tong, Synthesis, characterization and electrochemical behavior of cationic iron porphyrin intercalated into layered niobate, Microporous Mesoporous Mater. 151 (2012) 325.
[53] N-n. Wang, Y-x. Lan, J. He, R. Dong, J-s. Hu, Synthesis and characterization of ktinbo 5 nano-particles by novel polymerizable complex method, Bull. Korean Chem. Soc. 34 (2013) 2737-2740.
[54] J. He, A.Xu, L.Hu, N.Wang, W.Cai, B.Wang, J.Hu, Z.Li, Layered ktinbo5 photocatalyst modified with transitional metal ions (Mn^{2+}, Ni^{2+}): Investigation of microstructure and photocatalytic reaction pathways for the oxidation of dimethyl sulfide and ethyl mercaptan, Powder Technol. 270 (2015)154-162.
[55] S-H. Byeon, H-J. Nam, Neutron diffraction and ft-raman study of ion-exchangeable layered titanates and niobates, Chem. Mater. 12(6) (2000) 1771-1778.
[56] M. Fang, C.H., Kim, G.B. Saupe, H-N. Kim, C.C. Waraksa, T. Miwa, A. Fujishima, T.E. Mallouk, Layer-by-layer growth and condensation reactions of niobate and titanoniobate thin films, Chem. Mater. 11(6) (1999)1526-1532.